Peer-reviewed version available at *Materials* **2020**, *13*, 2825; doi:10.3390/ma13122825

Article

Hot Deformation Behavior and Microstructure Evolution of the Dual-Scale SiCp/A356 Composites Based on Optimal Hot Processing Parameters

Yahu Song [1,3], Aiqin Wang [1,*] , Douqin Ma [2], Jingpei Xie [1], Zhen Wang [1] and Liu Pei[1]

[1] School of Material Science and Engineering, Henan University of Science and Technology, Luoyang 471023, China; syh198703@163.com;aiqin_wang888@163.com; jingpeixie@163.com; 582030591@qq.com; liupei_hkd@163.com

[2] Provincial and Ministerial Co-construction of Collaborative Innovation Center for Non-ferrous Metal New Materials and Advanced Processing Technology, Luoyang 471023, China; madouqin1987@163.com

[3] CITIC Heavy Industries CO., Ltd, Henan Luoyang 471039, China; syh198703@163.com

* Correspondence: aiqin_wang888@163.com; Tel.: +86-13938881511

Abstract: Hot deformation at elevated temperature is essential to densify the particle reinforced Aluminum matrix composites (AMCs) and improve their performance. However, hot deformation behavior of the AMCs is sensitive to the variation of hot processing parameters. In this paper, optimal processing parameters of the dual-scale SiCp/A356 composites was determined to explore the control strategy of the microstructure. Hot compression tests were conducted at the temperature ranging from 460 to 520℃ under strain rates from 0.01 to 5 s^{-1}. Constitutive equation and processing maps were presented to determine the hot processing parameters. Microstructure evolution of the dual-scale SiCp/A356 composites was analyzed. The strain rate of 0.62 ~ $5s^{-1}$ and deformation temperature of 495 ~ 518℃ is suitable for the hot processing. The number of DRX grains in the "safe" domains is larger and the dislocation density is lower compared to those of instability domains. DRX particles mainly occurred around SiC particles. The presence of SiC particles can promote effectively the DRX nucleation, which result in that the dynamic softening mechanism of the dual-scale SiCp/A356 composites is dominated DRX.

Keywords: dual-scale SiCp/A356 composites; hot deformation behavior; microstructure; constitutive equation; processing map

1. Introduction

Due to their low density and expansion coefficient, high specific strength and specific modulus, good high temperature performance and wear resistance, SiC particle reinforced Al-Si matrix (A356, A357) are appropriate materials for weight reduction in the field of automotive industry and other engineering applications [1-4]. Traditionally, the SiCp/Al-Si matrix composite is usually fabricated using either the micro-sized or nano-sized SiC particles. However, the comprehensive properties of these single sized SiCp/Al-Si composites are hard to achieve ideal condition, such as, the enhancement of the strength for Al-Si matrix composites caused by micro-sized SiC particles are usually at the expense of sacrificing ductility, although the nano-sized SiC particles could retain the plasticity of Al alloys, the enhancement of strength and wear resistance for composites are not remarkable. In recent years, it has been found that the simultaneous introduction of micro-and nano-sized particles into the Al-Si alloy could significantly improve the comprehensive properties with the idea of micro-sized SiC particles help in enhancing the hardness, strength and wear resistance, while the nano-sized SiC particles help in retaining the plasticity [5-7].

It is well known that metal matrix composite often needs secondary thermo-mechanical processing such as hot forging, hot extrusion and hot rolling before they are used as structural or functional material in industry, because the secondary thermo-mechanical processing could effectively regulate the mechanical properties and microstructure of composites [8-10]. In this case,

Peer-reviewed version available at Materials 2020, 13, 2825; doi:10.3390/ma13122825

the hot deformation behavior of composites should be strictly controlled during the secondary thermo-mechanical processing due to its effect on microstructure and workability of composites. In recent years, there are many research work have been conducted to study the hot deformation behavior of either micro-sized or nano-sized SiCp/Al composite [11-18], and the results showed that the deformation behavior of SiCp/Al composites is greatly influenced by the SiC particle condition (particle size, distribution and volume).

Dynamic recrystallization (DRX) is an important phenomenon for controlling microstructure and mechanical properties in hot working. Its effect on the microstructure and properties of the material after processing and determinations of hot flow behavior are quite important in the modeling of the hot working processes. Generally, DRX rarely occurs in aluminum alloy and its composites since the high stacking fault energy of these materials commonly leads to the climb and cross-slip of the dislocation [19]. In fact, DRX occurred during hot deformation of aluminum alloys [18,20]. And it is related to the size and distribution of SiC particles and the hot deformation conditions [21-23]. The non-uniform deformation areas around the large and widely spaced micron SiC particles with high density dislocation and the large lattice orientation difference with the matrix leading to the particle induced nucleation (PSN). Dynamic recrystallization nucleation was induced. However, the nano SiC particles can improve the uniformity and stability of dislocation distribution in the hot deformation process. And it reduces the average orientation difference between subgrains. The dynamic recrystallization nucleation can be suppressed. However, the research of hot deformation behavior of particle reinforced AMCs is mainly focused on single micron or nano reinforced particles [24-26].

Based on the above analysis, hot deformation behavior of the dual-scale SiCp/A356 composites was clarified using the hot compression flow curves in the present work. Constitutive equation and processing maps were presented to determine the hot working constants. Microstructure evolution of the dual-scale SiCp/A356 composites was analyzed. Furthermore, hot deformation behavior was analyzed by the dislocation particulate interactions model.

2. Materials and Methods

The dual-scale SiCp/A356 composite was prepared via powder metallurgy（PM） by mixing micro-sized SiC powder with the average size of 10 μm, nano-sized SiC powder with the average size of 80 nm, and A356 alloy powder with the average size of 7 μm. The content of micro- and nano-sized SiC particles in the composite was 2 vol.% and 13 vol.%, respectively. The elemental compositions of the original A356 alloy powder were shown in Table.1.

Table 1. Chemical composition of the A356 alloy powder (wt. %)

Element	Si	Mg	Cu	Fe	Al
Weight Percent	7.0	0.3	0.1	0.1	Others

Preparation process of composite was as follows: Firstly, the nano-sized SiC particles were mixed with A356 aluminum alloy powder by the QM-BP planetary ball mill at a rotation speed of 150 r/min for 12 h, then the micro-sized SiC particles were mixed with the composite powders with the same process. Secondly, the mixed powders were pressed by using a 500T four-column hydraulic press at 500MPa for 60 min, and then the cold-pressed samples were sintered in an argon atmosphere protected sintering furnace (SG-GL1200 type) at 550℃ for 4h. After that, the sintered samples were hot extruded using an horizontal extruder(XJ-500 type) at 500℃ with an extrusion ratio of 15:1 and extrusion speed of 1mm/s. Finally, the composite was annealed in the gas protected sintering furnace at 300℃ for 2 h. Microstructure of composites was analyzed with the optical microscope (OM, Axiovert 200MAT) and transmission electrical microscope (TEM, JEM-2100). The dual-scale SiCp/A356 composites comprise black micro SiC particles and gray Si phase (Figure. 1(a)). The nano SiC particles were further examined in detail by TEM (Figure. 1(b)). Nano SiC particles are uniform distributed on the Al matrix.

Peer-reviewed version available at Materials 2020, 13, 2825; doi:10.3390/ma13122825

At last the composite was processed into small cylindrical samples with the size of Φ8mm × 12mm by wire cutting, and a small hole of Φ0.5mm × 2.5mm was machined on the side of the samples to install the thermocouple. Hot compression tests were taken by Gleeble-1500D thermal simulator at the temperature of 460, 480, 500, 520℃ and the strain rates of 0.01, 0.1, 1, 5 s^{-1}, respectively. True strain value was set as 0.7. Figure 2 show the hot deformation process diagram in the present work.

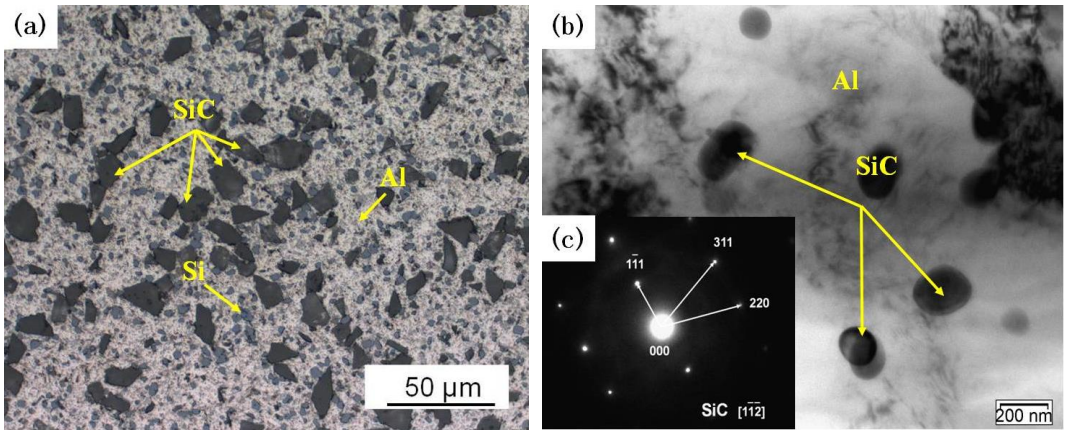

Figure 1. (a) Optical microstructure and (b) TEM images of the composites ;(c) Diffraction pattern of the nano SiC.

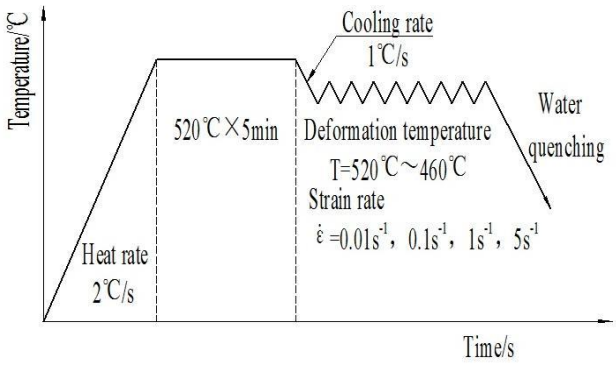

Figure 2. The hot deformation process diagram

3. Results

3.1. Stress-strain curves

Stress-strain curves are shown in Figure 3. Most of curves exhibit typical DRX behavior with a single peak stress followed by a gradual fall towards a steady state stress [27]. The main softening mechanism of the dual-scale SiCp/A356 composites is DRX. When the samples deformed at the strain rate of 0.1 s^{-1}, the cyclic peaks DRX can be observed (Figure 3(b)). This is due to the recrystallization soften effect cannot be balanced with the new work hardening because of the low dislocation increment rate. The peak stress increased when the strain rate increased and the deformation temperature decreased (Table 2). Because the higher temperature and the smaller the train rate, the deformation resistance of the material is smaller. And it is easier for the composites to achieve steady deformation at highe temperature and low strain rate. For example, when the temperature is 520℃ and the strain rate is 0.01 s^{-1}, the DRX is not obvious. A plateau in the stress–strain curve is achieved (Figure 3(a)).

Peer-reviewed version available at Materials 2020, 13, 2825; doi:10.3390/ma13122825

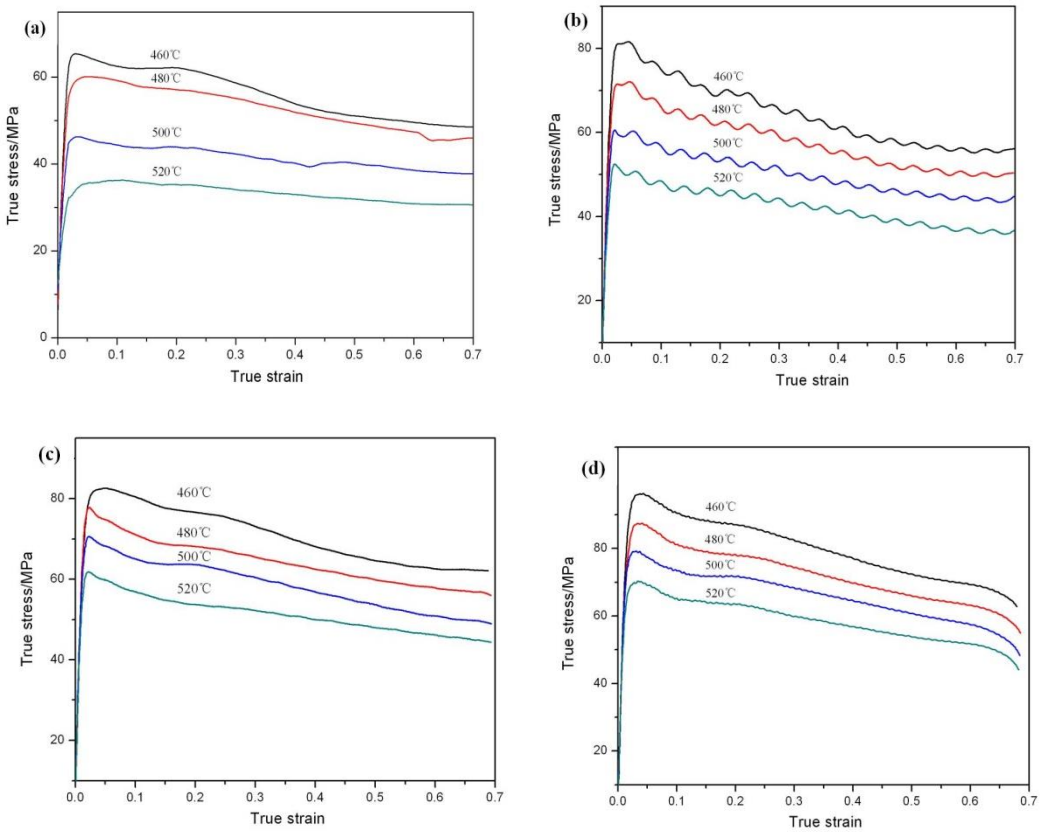

Figure 3. True strain–stress curves at different strain rates: (a) 0.01 s^{-1}; (b) 0.1 s^{-1}; (c) 1 s^{-1}; (d) 5 s^{-1}

Table 2. Peak stress at different hot processing parameters

Strain rate /s^{-1}	Temperature /℃			
	460	480	500	520
0.01	65.37618	60.13297	46.28657	36.30753
0.1	81.61172	72.08328	60.55818	52.44261
1	82.60639	77.8271	70.65215	61.87151
5	96.25351	87.496	79.18527	70.3212

3.2. Constitutive equation

Hot deformation behavior is a thermal activation process. Constitutive equations were used to calculate the activation energy(Q). The power law description of stress (Equation 1) is preferred for relatively low stresses. Conversely, the exponential law (Equation 2) is only suitable for high stresses [28,29]. However, the hyperbolic sine law (Equation 3) can be used for a wide range of temperatures and strain rates [30]. The Zener–Hollomon parameter (Z) is the temperature-compensated strain rate (Equation 4).

$$\dot{\varepsilon} = A_1\sigma^{n'}\exp(\frac{-Q}{RT}) \quad (\alpha\sigma \leqslant 0.8) \tag{1}$$

$$\dot{\varepsilon} = A_2\exp(\beta\sigma)\exp(\frac{-Q}{RT}) \quad (\alpha\sigma \geqslant 1.2) \tag{2}$$

$$\dot{\varepsilon} = A[\sinh(\alpha\sigma)]^n\exp(\frac{-Q}{RT}) \quad (\text{for all } \alpha\sigma) \tag{3}$$

Peer-reviewed version available at Materials 2020, 13, 2825; doi:10.3390/ma13122825

$$Z = \dot{\varepsilon}\exp(\frac{Q}{RT}) = A[\sinh(\alpha\sigma)]^n \quad (4)$$

where A_1、A_2、A、α、n、β and n' are material constant ($\alpha=\beta/n'$), R is the universal gas constant, T is the deformation temperatures (T is in K).

By taking natural logarithm from each side of Equations 1-3, the Equations 5-7 could be derived for the peak stress.

$$\ln\dot{\varepsilon} = \ln A_2 + n'\ln\sigma - \frac{Q}{RT} \quad (5)$$

$$\ln\dot{\varepsilon} = \ln A_1 + \beta\sigma - \frac{Q}{RT} \quad (6)$$

$$\ln\dot{\varepsilon} = \ln A - \frac{Q}{RT} + n\ln[\sinh(\alpha\sigma)] \quad (7)$$

When the temperature is certain, $n'$and β are the slopes of $\ln\dot{\varepsilon}$-lnσ and $\ln\dot{\varepsilon}$-σ curves, respectively. By taking partial derivative of Equation 3, the Equation 8 is obtained.

$$Q = R\frac{\partial\ln[\sinh(\alpha\sigma)]}{\partial(1/T)}\Big|_{\dot{\varepsilon}} \cdot \frac{\partial\ln\dot{\varepsilon}}{\partial\ln\sinh(\alpha\sigma)]}\Big|_T = nRK \quad (8)$$

Where n and K are the slopes of $\ln\dot{\varepsilon}$- ln[sinh(ασ)] and ln[sinh(ασ)] - 1/T curves, respectively.

It follows from Equations 5-6 that the slope of the plot of $\ln\dot{\varepsilon}$ against lnσ and the slope of the plot of $\ln\dot{\varepsilon}$ against σ can be used for obtaining the values of n′ and β, respectively (Figure 4 (a) and (b)). The value of σ takes the peak stress. By calculating the average values of the slopes of different straight lines, the average values of 12.78 and 0.1871; for n′and β can be obtained, respectively. This gives the value of $\alpha=\beta/n'$= 0.01464. According to Equation 7, the slope of the plot of $\ln\dot{\varepsilon}$ against ln[sinh(ασ)] and the slope of the plot of ln[sinh(ασ)] against 1000/T can be used for obtaining the value of n and K, respectively (Figure 4 (c) and (d)). The average value of n and K were determined as 10.2816 and 5.1711, respectively. According to Equation 8, the activation energy can be calculated($Q= nRK$ =442.03kJ/mol).

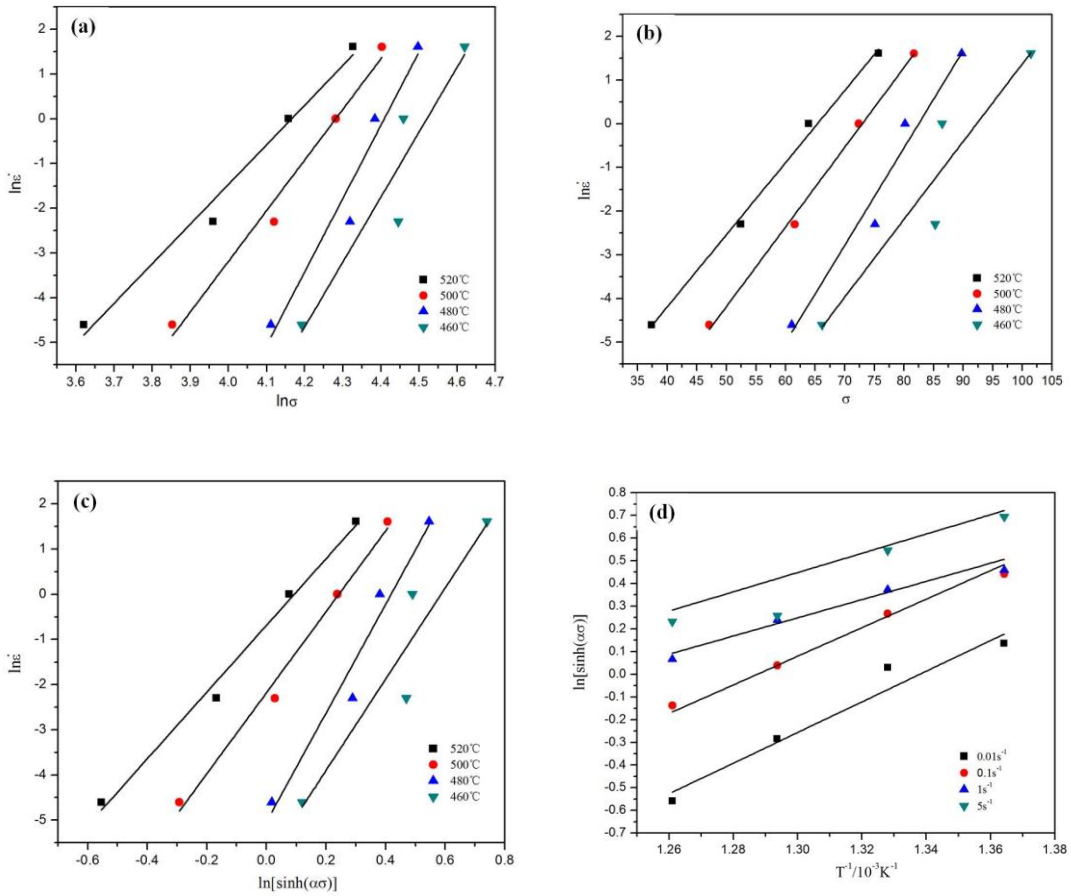

Peer-reviewed version available at Materials 2020, 13, 2825; doi:10.3390/ma13122825

Figure 4 Plots used for calculation of hot processing parameters

By taking natural logarithm from each side of Equation 4, the Equation 9 could be derived. According to the Equations 8-9, the value of LnZ under the different T and $\dot{\varepsilon}$ can be obtained (Table 3). It follows from Equation 9 that the intercept on lnZ axis of the plot of lnZ against ln[sinh($\alpha\sigma$)] can be used for obtaining the value of ln$A$. The value of A was determined as A=$e^{66.93}$. It can be seen in Figure 5 that the plot of lnZ against ln[sinh($\alpha\sigma$)] are in good agreement with the test data of SiCp/A356 composites under different deformation conditions (Table 3).

$$\ln Z = \ln \dot{\varepsilon} + Q/RT = \ln A + n \ln[\sinh(\alpha\sigma)] \tag{9}$$

Table 3 The value of lnZ

$\dot{\varepsilon}$/s^{-1}	T /℃			
	460	480	500	520
0.01	67.92850207	66.00197691	64.17514257	62.44045625
0.1	70.23108716	68.304562	66.47772766	64.74304134
1	72.53367225	70.60714709	68.78031276	67.04562643
5	74.14311016	72.216585	70.38975067	68.65506434

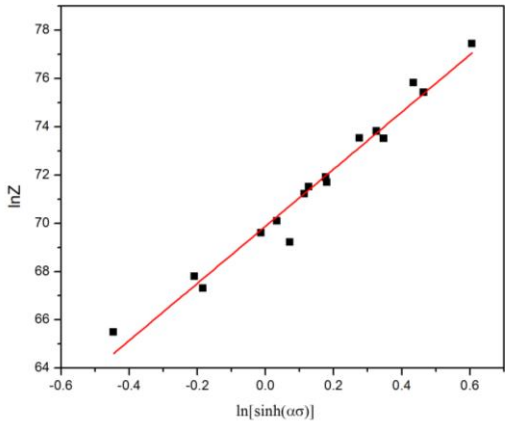

Figure 5 Plots used to derive the constitutive equations

Taking the values of n, α, A and Q into Equation 3, the constitutive equation of SiCp / A356 composites is obtained as follows:

$$\dot{\varepsilon} = e^{66.93} \times [\sinh(0.01464\sigma)]^{10.2816} \exp(-\frac{442.03}{8.314T})$$

The calculated peak stress value by constitutive equation is compared with the tested value (Figure 6(a)). And the fitting degree is quantitatively evaluated by using the statistical parameters such as linear correlation coefficient (R) and average relative error (AARE) (Equations 9-10). The results show that the correlation coefficient is 0.951(R > 0.95) and the average relative error is 4.26% (AARE < 5%). It indicated the constitutive equation has high fitting degree and applicability (Figure 6(b)).

Peer-reviewed version available at Materials 2020, 13, 2825; doi:10.3390/ma13122825

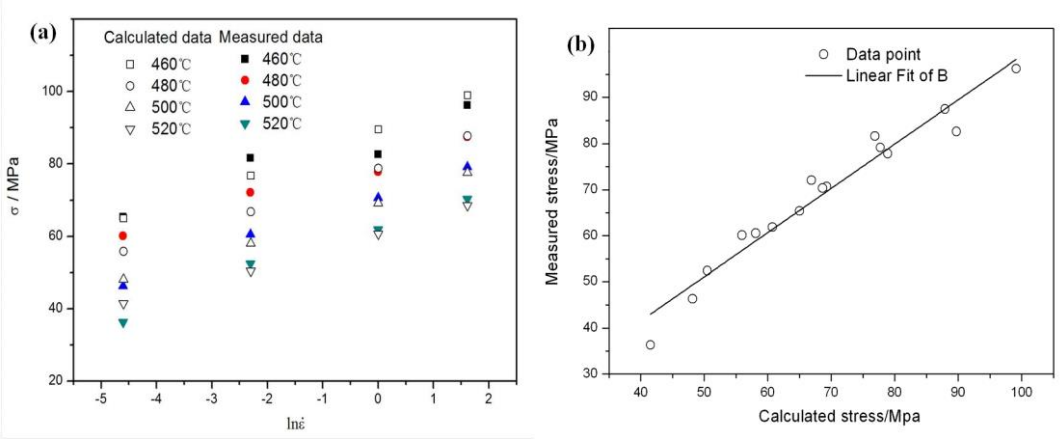

Figure 6 The comparison of calculated and measured values of peak stress for the dual-scale SiCp/A356 composites

$$R = \frac{\sum_{i=1}^{N}(E_i - \bar{E})(P_i - \bar{P})}{\sqrt{\sum_{i=1}^{N}(E_i - \bar{E})^2 \sum_{i=1}^{N}(P_i - \bar{P})^2}} = 0.951 \tag{10}$$

$$AARE = \frac{1}{N}\sum_{i=1}^{N}\left|\frac{E_i - P_i}{E_i}\right| \times 100\% = 4.26\% \tag{11}$$

Where, E_i is the test stress value, P_i is the calculated stress value, $\bar{E}$ and $\bar{P}$ is the average test value and the calculated value of the stress, respectively. N is the number of all data points.

3.3. Processing maps

Processing map is established mainly based on dynamic material model (DMM)[31], which is composed of power dissipation diagram and rheological instability diagram. It is used to describe the safe domains and instability domains. The power dissipation diagram reflects the change of microstructure under certain deformation temperature and strain rate, such as dynamic recovery, dynamic recrystallization and super plasticity, which is generally expressed by power dissipation factor η [32](Equation 12).

$$\eta = \frac{2m}{m+1} \tag{12}$$

Where m is the strain rate sensitive factor. Under a certain T and $\dot{\varepsilon}$, m can be expressed as Equation 13.

$$m = \frac{\partial \ln \sigma}{\partial \ln \dot{\varepsilon}} \tag{13}$$

The cubic spline function is used to fit the relation curve between lnσ and ln $\dot{\varepsilon}$, and then the slope of the spline function is the value of m. The value of η can be obtained from Equation 12. The contour curve of η is drawn in the T-ln $\dot{\varepsilon}$ plane. The result shows that the higher of η, the better the hot performance of the materials. However, the high η does not completely indicate the good hot performance due to the value of η may be very high in the flow instability region. So it is necessary to clarify the flow instability region accurately [33].

According to the principle of irreversible thermodynamic extreme value, the criterion of continuous instability plastic deformation of materials can be expressed by dimensionless parameters $\xi(\dot{\varepsilon})$ [34] (Equation 14):

Peer-reviewed version available at Materials 2020, 13, 2825; doi:10.3390/ma13122825

$$\xi(\dot{\varepsilon}) = \frac{\partial \ln\left(m/(m+1)\right)}{\partial \ln \dot{\varepsilon}} + m < 0 \quad (14)$$

Therefore, the instability condition is also related to m. The region ($\xi(\dot{\varepsilon}) < 0$) is the rheological instability diagram. When the power dissipation diagram and rheological instability diagram are superposed, it is the processing map (Figure 7). The gray area is the rheological instability area, and the white area is the safe processing area. It can be seen that there are three instability domains: the region with strain rate of 0.62 ~ 5s^{-1} and deformation temperature of 464 ~ 495℃; the strain rate of 0.01 ~ 0.03s^{-1} and deformation temperature of 460 ~ 512℃; and the strain rate of 1 ~ 5s^{-1} and deformation temperature of 518 ~ 520℃. In addition, there are two safe processing areas: the area with strain rate of 0.62 ~ 5s^{-1} and deformation temperature of 495 ~ 518℃(DOMI) and the area with strain rate of 0.03 ~ 0.62$s^{-1}$and deformation temperature of 460 ~ 520℃(DOMII). The DOMI with the highest η is the best for the hot processing for dual-scale SiCp/A356 composites. When the deformation temperature is 500℃, no matter how the strain rate changes in the range of 0.03 ~ 5s^{-1}, it is suitable for the hot processing.

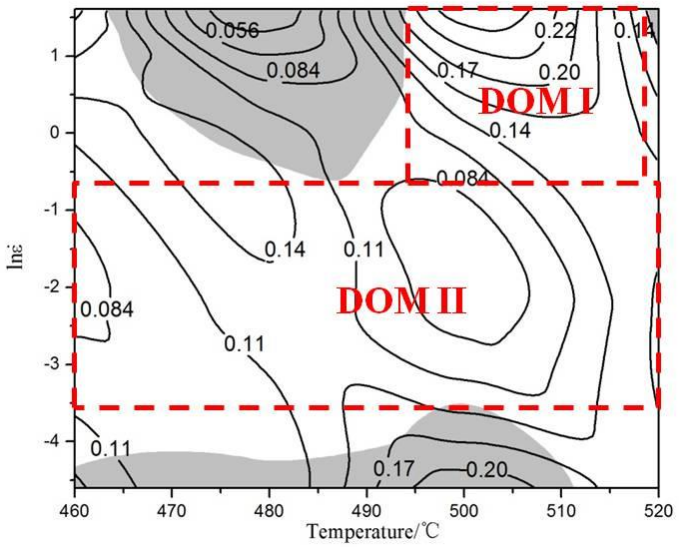

Figure7 Processing maps of the dual-scale SiCp/A356 composites at the strain of 0.5 s^{-1}

3.4. Microstructure analysis

Figure 8 shows the effects of deformation temperature on the microstructure when the strain rate is 1s^{-1}. When the temperatures is 460℃ there are obviously disordered and entangled dislocation lines in the matrix (Figure 8(a)). When the deformation temperature is 480℃, dynamic recrystallized grains are generated with clear grain boundaries but part of the grains in a curved shape(Figure 8(b)). At the same time, a large number of dislocation structures can be seen inside and outside the recrystallized grains. It indicated that the dynamic recrystallized grains are not fully grown. When the deformation temperature rises above 500℃ (Figure 8(c and d)), the grain boundary of the dynamic recrystallized grain is straight and clear, which is obvious isometric grain. And the dislocation density in the grain is very low. It indicated that the dynamic recrystallized grain has grown sufficiently at 500℃. Figure 9 shows the effects of strain rate on the microstructure when the deformation temperature is 500℃. At a high strain rate, the growth of dynamic recrystallized grains is inhibited, and there are some scattered dislocations in the grains (Figure 9(a and b)). At a low strain rate, dislocation density decreases, grain boundary becomes clear and sharp, and recrystallized grain size increases (Figure 9(c and d)).

Peer-reviewed version available at Materials 2020, 13, 2825; doi:10.3390/ma13122825

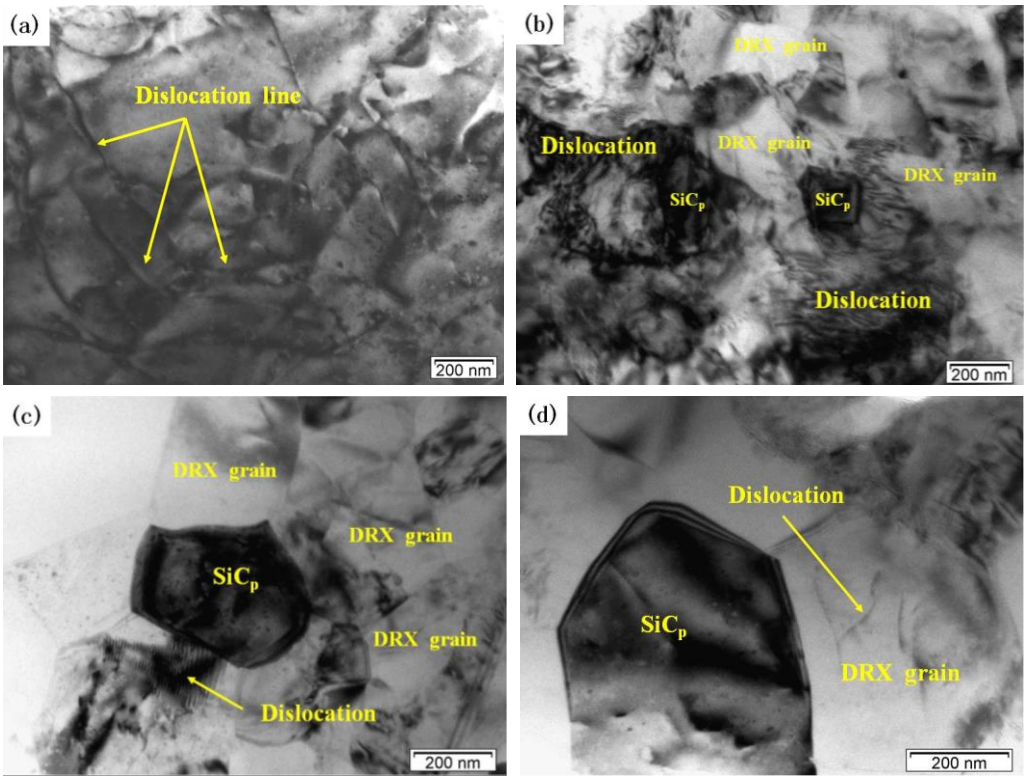

Figure. 8 TEM images of the dual-scale SiCp/A356 composites deformed at the strain rate of $1s^{-1}$ and different deformation temperature (a) 460℃; (b) 480℃; (c) 500℃; (d) 520℃

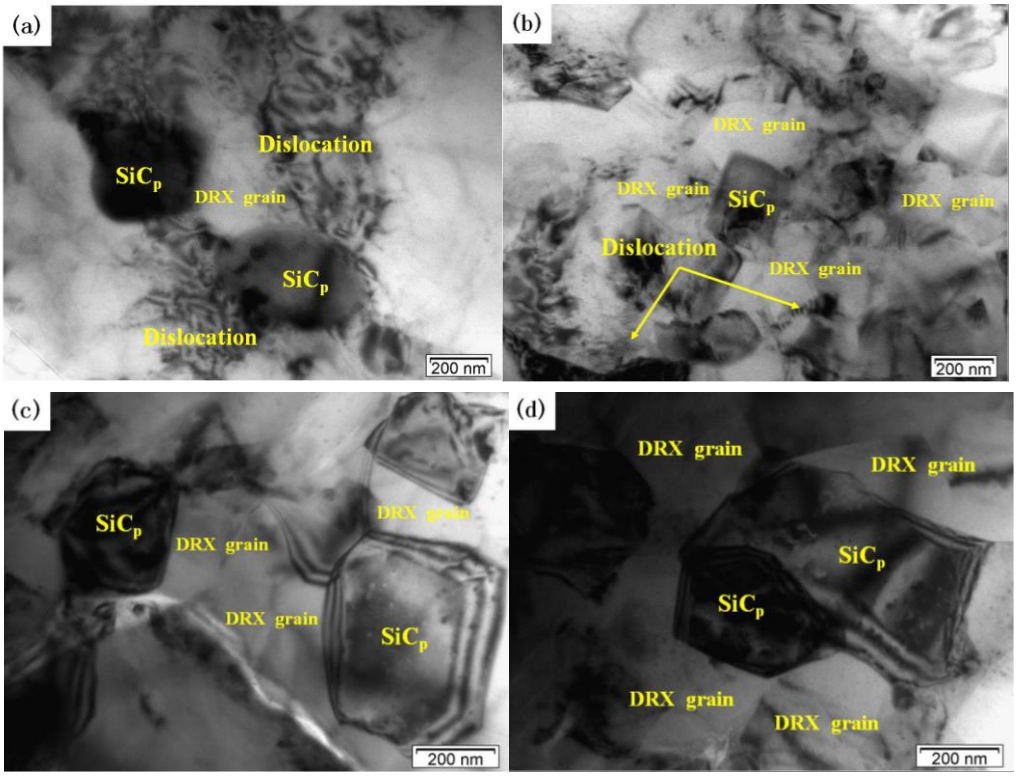

Figure. 9 TEM images of the dual-scale SiCp/A356 composites deformed at 500℃ and different strain rates: (a) $5s^{-1}$; (b) $1s^{-1}$; (c) $0.1s^{-1}$; (d) $0.01s^{-1}$

With the increase of deformation temperature and the decrease of the strain rate, dislocation density around the SiC particles gradually reduce and the dislocation destruction and rearrangement are more abundant due to the easy climbing and slip of the dislocation. Moreover, the dynamic recrystallization grain size grew up gradually, and the boundary gradually clear and

Peer-reviewed version available at Materials 2020, 13, 2825; doi:10.3390/ma13122825

straight [35,36]. DRX particle size increases significantly when the deformation temperature is up to 520 ℃ from 500 ℃. It shows that the effect of deformation temperature on the dynamic recrystallization of materials is more obvious than that of strain rate. This is also consistent with the optimal processing conditions of materials, where the temperature range is narrow (495~518 ℃) and the strain rate range is wide (0.62~5s^{-1}) (Figure 7).

DRX particles mainly occur around SiC particles. So, the presence of SiC particles can promote effectively the DRX nucleation, The number of DRX grains in the "safe" domains (Figure8c and Figure9c) is larger and the dislocation density is lower compared to those of instability domains. The typical microstructural characteristics of the "safe" domains correspond to the SiC particles and hot processing parameters.

3.5. Hot deformation behavior

Hot deformation behavior of the dual-scale SiCp/A356 composites can be explained by model of dislocation particulate interactions (Figure 10). In the process of the hot deformation, the dislocation in the aluminum matrix slips under the action of the external stress, while SiC particles as a non-deformable phase is an obstacle to dislocation motion. When the dislocation moves to the particle, stress concentration is generated. The stress also can be relaxed due to the climbing of the dislocation. Whether or not the dislocation will accumulate at the particle and how much it accumulates depends on the rate of the dislocation arriving at the particle (R1) and the climbing rate of the dislocation (R2). The n is used to represent the dislocation accumulation at the particle, the following functional relationship exists (Equation 15):

$$N=f（R1，R2） \quad (15)$$

Where R1 is related to the strain rate during the hot deformation, R2 is related to the deformation temperature, particle size and deformation mechanism. When the value of R2 is greater than the value of R1, the dislocation will not accumulate around the SiC particle (Figure 10c). The material will have a lower work-hardening rate and flow stress. When the value of R2 is smaller than the value of R1, the dislocation will accumulate around the SiC particle (Figure 10d). A complex dislocation structure will be formed at the particle with the increase of the accumulation degree. The material shows high machining hardening rate and flow stress [24].

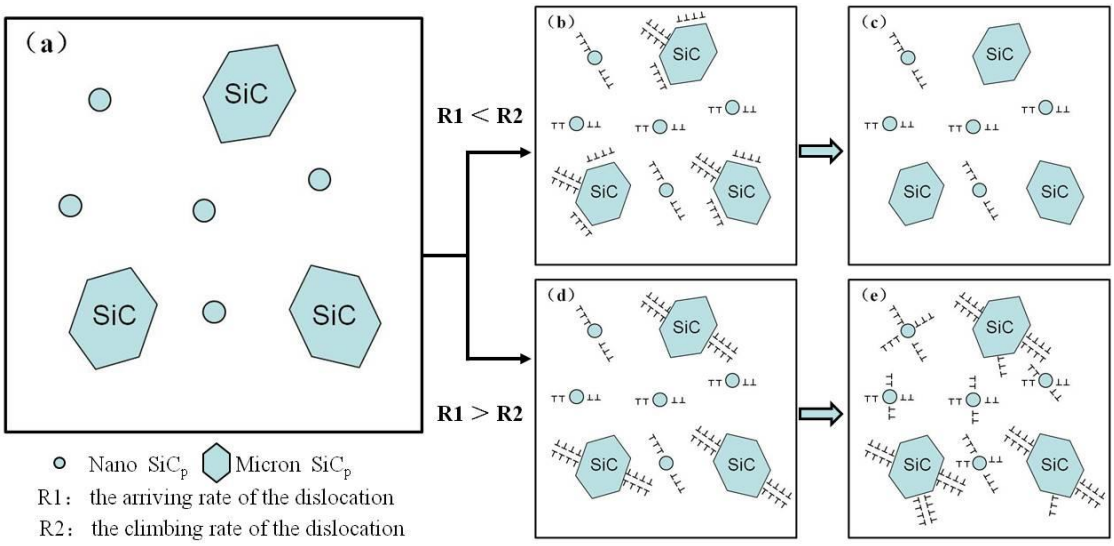

Figure.10 Model of dislocation particulate interactions of the dual-scale SiCp/A356 composites

At the early stage of deformation, R1 can be considered to be constant for the given initial rate. The value of R2 is smaller than the value of R1. At this time, with the increase of deformation degree, the dislocation accumulation at the SiC particles leads to the increase of the hardening rate and stress, which is more significant at low temperature deformation (Figure. 3a). With the further

Peer-reviewed version available at Materials 2020, 13, 2825; doi:10.3390/ma13122825

increase of deformation degree, the process of DRX occurs. At this time, the value of R2 increases and the dislocation at the SiC particle plugging area gradually tends to maintain a stable dislocation density. At this time, the flow stress tends to be stable. It is consistent with the stress–strain curve in Figure 3. With the increase of the deformation temperature (the value of R2 increases), the dislocation density around the SiC particle decreased, so the peak stress decreased. While, with the increase of the strain rate (the value of R1 increases), the dislocation density at the particle increased, so the peak stress of the material increased. It is consistent with the peak stress in Table 2. Although, it is proposed that aluminum and its composites are difficult to produce DRX. Since, the climb and cross-slip of the dislocation are easy due to the high stacking fault energy of this kind of materials. And the dual-scale SiCp/A356 composites showed higher Q compared to the A356 and its composites [18]. The addition of SiC particles promotes dislocation pile-up and DRX nucleation due to PSN. The main softening mechanism of the dual-scale SiCp/A356 composites is DRX. And it is indicated that the dual-scale SiCp/A356 composites can obtain a homogenous ultrafine grained structure via hot deformation.

4. Conclusions

Hot deformation behavior and the corresponding microstructures of the dual-scale SiCp/A356 composites were investigated in the temperature range of 460~520℃ and the strain rate range of 0.01~5s^{-1}. The following conclusions have been drawn.

(1) Sress–strain curves showed typical DRX with a single peak stress followed by a gradual fall towards a steady state stress. Peak stress decreased with the increase of deformation temperature and the decrease of strain rate.

(2) The average deformation activation energy was 442.03kJ/mol. The correlation coefficient R for linear regression of constitutive model was 0.951, which indicated the high accuracy of this model. The constitutive equation was expressed as: $\dot{\varepsilon} = e^{66.93} \times [\sinh(0.01464\sigma)]^{10.2816} \exp(-\frac{442.03}{8.314T})$.

(3) There are two "safe" domains based on the processing maps: one is at temperature of 495 ~ 518℃and strain rate of 0.62 ~ 5s^{-1}; another is at temperature of 460 ~ 520℃and strain rate of 0.03 ~ 0.62s^{-1}. When the temperature of 495 ~ 518℃and strain rate of 0.62 ~ 5s^{-1} is suitable for the hot processing of dual-scale SiCp/A356 composites.

(4) The deformed microstructures at the corresponding processing parameters mainly exhibit DRX. The number of DRX grains in the "safe" domains is larger and the dislocation density is lower compared to those of instability domains. The typical microstructural characteristics of the "safe" domains correspond to the SiC particles and hot processing parameters.

(5) DRX particles mainly occur around SiC particles. The presence of SiC particles can promote effectively the DRX nucleation, which result in that the dynamic softening mechanism of the dual-scale SiCp/A356 composites is dominated DRX.

Author Contributions: Conceptualization, Yahu Song and Aiqin Wang; Data curation, Yahu Song; Formal analysis, Yahu Song; Funding acquisition, Aiqin Wang; Investigation, Yahu Song, Aiqin Wang, Douqin Ma, Jingpei Xie, Zhen Wang and Liu Pei; Methodology, Zhen Wang; Writing – original draft, Yahu Song; Writing – review & editing, Aiqin Wang and Jingpei Xie.

Funding: This research was funded by the National Natural Science Foundation of China (grant no. 51771070)

Conflicts of Interest: The authors declare no conflict of interest.

References

1. Wu, C.C.; Gao, T, Liu; X.F. In-situ SiC reinforced Si-SiC 3D skeletons in SiC/Al-Si composites. *J. Alloy. Compd.* **2019**, 810, 151730. (doi: 10.1016/j.jallcom.2019.151730)
2. Lee, H.; Sohn, S.S.; Jeon, C.; Jo, I.; Lee, S.K.; Lee, S. Dynamic compressive deformation behavior of SiC-particulate-reinforced A356 Al alloy matrix composites fabricated by liquid pressing process. *Mater. Sci. Eng. A.* **2017**, 680, 368-377. (doi: 10.1016/j.msea.2016.10.102)

Peer-reviewed version available at Materials 2020, 13, 2825; doi:10.3390/ma13122825

3. Yuan, D.; Yang, X.; Wu, S.S.; Lv, S.L.; Hu, K. Development of high strength and toughness nano-SiCp/A356 composites with ultrasonic vibration and squeeze casting. *J. Mater. Process. Tech.* **2019**, 269, 1-9. (doi: 10.1016/j.jmatprotec.2019.01.021)
4. Ravi Kumar, N. V.; Ramachandra Rao, N.; Gokhale, A. A. Effect of SiC particle content on foaming and mechanical properties of remelted and diluted A356/SiC composite. *Mater. Sci. Eng. A.* **2014**, 598, 343-349. (doi: 10.1016/j.msea.2014.01.050)
5. Lakshmikanthan, A.; Bontha, S.; Krishna, M.; Koppad, P.G.; Ramprabhu, T. Microstructure, mechanical and wear properties of the A357 composites reinforced with dual sized SiC particles. *J. Alloy. Compd.* **2019**, 786, 570-580. (doi: 10.1016/j.jallcom.2019.01.382)
6. Avinash, L.; Prabhu, T.R.; Bontha, S. The effect on the dry sliding wear behavior of gravity cast A357 reinforced with dual size silicon carbide particles. *Appl. Mech. Mater.* **2016**, 829, 83-89. (doi: 10.4028/www.scientific.net/AMM.829.83)
7. Zhang, Q.; Wu, G.; Sun, D.; Chen, G.; Jiang, L. Microstructure and thermal conduction properties of an Al-12Si matrix composite reinforced with dual sized SiC particles. *J. Mater. Sci.* **2004**, 39, 303-305. (doi: 10.1023/B:JMSC.0000007761.85651.d6)
8. Kai, X.Z.; Zhao, Y.T.; Wang, A.D; Wang, C.M.; Mao, Z.M. Hot deformation behavior of in situ nano ZrB_2 reinforced 2024Al matrix composite. *Compos Sci. Technol.* **2015**, 116, 1-8. (doi:10.1016/j.compscitech.2015.05.006)
9. Xiao, P.; Gao, Y.M.; Xu, F.X.; Yang, S.S.; Li, Y.F.; Li, B.; Zhao, S.Y. Hot deformation behavior of in-situ nanosized TiB_2 particulate reinforced AZ91 Mg matrix composite. *J. Alloy. Compd.* **2019**, 798, 1-11. (doi: 0.1016/j.jallcom.2019.05.244)
10. Cao, Y.K.; Liu, Y.; Li, Y.P.; Liu, B.; Xu, R.J. Hot deformation behavior of nano-sized TiB reinforced Ti-6Al-4V metal matrix composites. *Mech. Mater.* **2019**, 141, 103260. (doi: 10.1016/j.mechmat.2019.103260)
11. Cheng, M.Y.; Hao, S.M.; Xie, J.P.; Wang, A.Q.; Ma, D.Q. Hot deformation behavior of SiC_p/Al-Cu composite. *J. Mater. Eng.* **2017**, 45, 17-23. (doi: 10.11868/j.issn.1001-4381.2015.000528)
12. Chen, S.; Teng, J.; Luo, H.B.; Wang, Y.; Zhang, H. Hot deformation characteristics and mechanism of PM 8009Al/SiC particle reinforced composites. *Mater. Sci. Eng. A.* **2017**, 697, 194-202. (doi: 10.1016/j.msea.2017.05.016)
13. Hao, S.M.; Xie, J.P.; Wang, A.Q.; Wang, W.Y.; Li, J.W.; Sun, H.L. Hot deformation behaviors of 35% SiC_p/Al metal matrix composites. *T. Nonferr. Metal. Soc.* **2014**, 24, 2468-2474. (doi: 10.1016/s1003-6326(14)63372-0)
14. Deng, K.K.; Li, J.C.; Xu, F.J.; Nie, K.B.; Liang, W. Hot deformation behavior and processing maps of fine-grained SiCp/AZ91 composite. *Mater. Design.* **2015**, 67, 72-81. (doi: 10.1016/j.matdes.2014.11.006)
15. Sun, Y.L.; Xie, J.P.; Hao, S.M.; Wang, A.Q.; Liu, P.; Li, M. Dynamic recrystallization model of 30% SiCp/Al composite. *J. Alloy. Compd.* **2015**, 649, 865-871. (doi: 10.1016/j.jallcom.2015.04.111)
16. Wang, Z.; Wang, A.Q.; Xie, J.P.; Liu, P. Hot deformation behavior and strain-compensated constitutive equation of nano-sized SiC particle reinforced Al-Si matrix composites. *Materials.* **2020**, 13, 1812. (doi: 10.3390/ma13081812)
17. Huang, Z.Y.; Zhang, X.X.; Xiao, B.L.; Ma, Z.Y. Hot deformation mechanisms and microstructure evolution of SiCp/2014Al composite. *J. Alloy. Compd.* **2017**, 722, 145-157. (doi: 10.1016/j.jallcom.2017.06.065)
18. Chen, X.R.; Fu, D.F.; Teng, J.; Zhang, H. Hot deformation behavior and mechanism of hybrid aluminum-matrix composites reinforced with micro-SiC and nano-TiB_2. *J. Alloy. Compd.* **2018**, 753, 566-575. (doi: https://doi.org/10.1016/j.jallcom.2018.04.223)
19. Mirzadeh, H.; Cabrera, J.M.; Prado, J.M.; Najafizadeh, A. Hot deformation behavior of a medium carbon microalloyed steel. *Mater. Sci. Eng. A.* **2011**, 528, 3876-3882. (doi: 10.1016/j.msea.2011.01.098)
20. Kai, X.Z.; Zhao, Y.T.; Wang, A.D.; Wang, C.M.; Mao, Z.M. Hot deformation behavior of in situ nano ZrB2 reinforced 2024Al matrix composite. *Compos. Sci. Technol.* **2015**, 116, 1-8. (doi: 10.1016/j.compscitech.2015.05.006)
21. Hao, S.M.; Xie, J.P.; Wang, A.Q.; Wang, W.Y.; Li, J.W. Hot Deformation Behavior and Processing Map of SiCp/2024Al Composite. *Rare Metal Mat. Eng.* **2014**, 43, 2912-2916. (doi: 10.1016/S1875-5372(15)60032-7)
22. Gangolu, S.; Gourav R.A.; Sabirov, I.; Kashyap, B.P.; Prabhu, N.; Deshmukh, V.P. Development of constitutive relationship and processing map for Al-6.65Si-0.44Mg alloy and its composite with B_4C particulates. *Mater. Sci. Eng., A.* **2016**, 655, 256-264.(doi: 10.1016/j.msea.2015.12.093)
23. Cheng, M.Y.; Hao, S.M.; Xie, J.P.; Wang, A.Q.; Mao, D.Q.; Sun, Y.L. Hot deformation behavior of SiC_p/Al-Cu composite. *J. Mater. Eng.* **2017**, 45, 17-23. (doi: 10.4028/www.scientific.net/AMR.1058.165)

Peer-reviewed version available at Materials 2020, 13, 2825; doi:10.3390/ma13122825

24. Zhao, M.J.; Liu, Y.; Bi, J. Hot deformation behavior of silicon car-bide particulate reinforced 2024 aluminum based composite. *Acta Metall. Sin.* **2003**, 39, 221-224. (doi: 10.3321/j.issn:0412-1961.2003.02.024)
25. Patel, A.; Das, S.; Prasad, B.K. Compressive deformation be-havior of al alloy (2014)–10wt.% SiC_p composite: effects of strain rates and temperatures. *Mater. Sci. Eng. A.* **2011**, 530, 225-232. (doi: 10.1016/j.msea.2011.09.078)
26. Huang, Z.Y.; Zhang, X.X.; Xiao, B.Y.; Ma, Z.Y. Hot deformation mechanisms and microstructure evolution of SiCp/2014Al composite. *J. Alloy. Compd.* **2017**, 722, 145-157. (doi: 10.1016/j.jallcom.2017.06.065)
27. Wei, H.L.; Liu, G.Q.; Xiao, X.; Zhang, M.H. Dynamic recrystallization behavior of a medium carbon vanadium microalloyed steel. *Mater. Sci. Eng. A.* **2013**, 573, 215-221. (doi: 10.1016/j.msea.2013.03.009)
28. Zener, C.; Hollomon, J.H. Effect of strain rate upon plastic flow of steel. *J. Appl. Phys.* **1944**, 15, 22-32. (doi: 10.1063/1.1707363)
29. Wang, Y.; Ling, D.L.; Law, C.C. A correlation between tensile flow stress and Zener-Hollomon factor in TiAl alloys at high temperatures. *J. Mater. Sci. Let.* **2000**, 19, 1185-1188. (doi: 10.1023/A:1006723629430)
30. Sellars, C.M.; Tegart, W.J. Hot workability. *Int. Mater. Rev.* **1972**, 17, 1-24. (doi: 10.1179/095066072790137765)
31. Xiong, Y.; Xiong, L.Y.; Zhang, L.F.; Chen, Z.G.; Wang, S.X.; Cai, D.Y. Hot deformation behavior and microstructure evolution of super alloy GH4199. *Trans. Nonferrous Met. Soc. China.* **2010**, 20, 655-661. (doi: 10.1016/S1875-5372(10)60130-0)
32. Chen, B.; Tian, X.L.; Li, X.L.; Lu, C. Hot Deformation Behavior and Processing Maps of 2099 Al-Li Alloy. *J. Mater. Eng. Perform.* **2014**, 23, 1929-1935. (doi: 10.1007/s11665-014-0955-2)
33. Guo, Y.J.; Deng, L.; Wang, X.Y.; Jin, J.S.; Zhong, W.W. Hot Deformation Behavior and Processing Maps of 7050 Aluminum Alloy. *Ad. Mate. Res.* **2013**, 815, 37-42. (doi: 10.4028/www.scientific.net/amr.815.37)
34. Liu, J.H.; Liu, J.S.; Xiong, Y.S.; He, W.W.; Zhang, P.; Liu, X.M. Hot deformation and processing maps of TC4-DT titanium alloy. *Rare Metal Mat. Eng.* **2013**, 42, 1674-1678. (doi: 10.1016/j.jallcom.2013.03.072)
35. Hu, H.E.; Zhen, L.; Zhong, B.Y.; Yang, L.; Chen, J.Z. Microstructure characterization of 7050 aluminum alloy during dynamic recrystallization and dynamic recovery. *Mater. Charact.* **2008**, 59, 1185-1189. (doi: 10.1016/j.matchar.2007.09.010)
36. Huang, X.D.; Zhang, H.; Han, Y.; Wu, W.X.; Chen, J.H. Hot deformation behavior of 2026 aluminum alloy during compression at elevated temperature. *Mater. Sci. Eng. A.* **2010**, 527, 485-490. (doi: 10.1016/j.msea.2009.09.042)